Analysis of Mounting Layouts for Improved Vibration Isolation Performance of an Automotive Cooling Module

UNDERGRADUATE HONORS THESIS

Presented in Partial Fulfillment of the Requirements for Graduation with Honors Research Distinction in the Department of Mechanical and Aerospace Engineering at The Ohio State University

By

Wenzhao Ye

Undergraduate Program in Mechanical Engineering

The Ohio State University

2017

Undergraduate Thesis Committee:

Dr. Jason Dreyer

Dr. Prasad Mokashi

Dr. Sandra Metzler

Abstract

An automotive cooling module plays an important role with respect to energy efficiency and dynamic performance of a vehicle. Many studies have focused on thermodynamic aspects of such cooling modules; however, increased demand for lighter weight structures and fuel-efficient vehicles requires a critical re-examination of their mounting schemes, specifically in terms of vibration isolation. Therefore, this research evaluates a representative automotive cooling module isolation system using both experimental and computational means to better understand how the mounting layout can be modified to reduce the transmission of dynamic forces from the module structure to the vehicle body. First, a lumped parameter model of a radiator-fan assembly is created in which incorporates commercially available radiator-fan assembly size and mounting layouts. Second, elastomeric mount stiffness and damping matrices are identified using a correlation between finite element analysis and dynamic bench experiments. Next, a laboratory experiment is designed and conducted to correlate the model for specific cases. Finally, the model is exercised under systematical changes of operating conditions and mounting configurations to quantify the isolation performance of the radiator-fan assembly. Results of this study quantify the effects on radiator isolation performance due to changes of lower isolator mount locations, stiffness, and damping properties. Increasing the stiffness through material hardness change can reduce transmitted vertical forces, however, could potentially increase transmitted lateral forces. Increasing lateral stiffness

independently through a geometric modification of isolator mounts can also reduce the transmitted lateral forces. Finally, increasing the mount material damping could also reduce both transmitted vertical and lateral forces. The tractable modeling approach from this study could potentially be used as a design tool to quickly scale the isolation systems for new vehicle architectures.

Dedication

Dedicated to the students at The Ohio State University.

Acknowledgements

I am grateful to my advisor Dr. Jason Dreyer, who has provided me with this precious undergraduate research opportunity. Dr. Dreyer has advised me throughout entire research process even after he left the faculty position at the Department of Mechanical and Aerospace Engineering and went to industry. Without his advising and encouraging, I could not have completed the first research project in my life.

I would also like to acknowledge the National Science Foundation, its Industry-University Cooperative Research Center on Smart Vehicle Concepts at OSU, and its industry and government sponsor organizations. I would also like to acknowledge Ram Ramesh for his technical advice on this project. Finally, I would like to thank Dr. Prasad Mokashi and Dr. Sandra Metzler for helping me, taking time reviewing my thesis, and serving as undergraduate thesis committee members.

Vita

September 2008	The High School Affiliated to Beijing Normal University
September 2011	Huazhong University of Science and Technology
August 2014	The Ohio State University

Fields of Study

Major Field: Mechanical Engineering

Topics: Dynamics and Vibrations

Table of Contents

List of Tables

List of Figures

List of Symbols

A	Surface area
B	Coordinate transformation
c	Viscous damping coefficient
C	Damping matrix
f	Force
F	Force amplitude
e	Eccentric radius
h	Convective heat transfer coefficient
I	Inertia
j	$\sqrt{-1}$
k	Stiffness
k_{air}	Thermal conductivity of air
K	Stiffness matrix
l	Length
m	Mass
m_e	Eccentric mass
Nu	Nusselt number
Pr	Prandtl number
q	Displacement vector
Q	Heat flow rate
r	Position vector

r	Normalized frequency
R	Reaction force
Re	Reynolds number
t	Time
T	Temperature
u	Fluid velocity
y, z	Translation coordinate
x	Displacement
X	Displacement amplitude

β	Proportional damping scaling with respect to stiffness matrix
Δr	Displacement vector
ζ	Damping ratio
ϕ	Phase angle
θ	Rotational coordinate
ν	Kinematic viscosity
ψ	Mode shape vector
ω	Angular frequency

Subscripts

0	Center of mass

$0i$	From point i to center of mass
i = 1,2,3,4	Mount number
k	Mode number
T	Transmitted
y	Lateral direction
z	Vertical direction
θ	Rotational direction

Operators

T	Transpose
..	Second derivative
.	First derivative
→	Vector
Bold	Matrix

Abbreviations

DOF	Degree-of-freedom
FRF	Frequency response function
ShA	Shore A hardness

1. Introduction

1.1. Motivation

The demand for fuel efficient vehicles is driving vehicle manufacturers to consider design concepts that integrate lighter weight structures as well as improved thermal management systems. Automotive cooling modules are become larger with the increased demand to remove heat from the engine to improve efficiency, while the structures around them are becoming lighter. These structures are also under increased requirements for strain energy management to absorb and divert energy from a crash impact away from or around the vehicle occupants. Lighter structures can reduce the energy consumption of vehicles; however, they can make the vehicle more sensitive to dynamic forces from powertrain vibrations or road inputs [1]. In addition, evolving designs applied to vehicle powertrains, such as high-performance engines, drivelines, transmissions, exhaust, and cooling modules, can also introduce new vibration and noise sources into the entire vehicle [1]. These vibration and noise sources as well as their interaction with vehicle structures can affect driver comfort or perceived quality of the vehicle, and inability to address such issues can render even the most efficient powertrain design unmarketable.

An automotive cooling module may consist of a radiator, mounting brackets and frame, elastomeric mounts, fans, hoses, condensers, and, in some cases, intercoolers. Although locations of these cooling modules in the front grills have not changed significantly in conventional automobiles, they have seen a trend of increased capactiy and reduced packaging space. Often the fan is mounted to the radiator structure, which is

mounted to the vehicle structure through elastomeric mounts. These mounting systems typically consist of four elastomeric mounts, which constrain the motion of the radiator within the engine compartment as well as provide vibration isolation between the radiator and the vehicle structure. Dynamic forces can be generated in a cooling module from unbalances in the rotating components and from transient speed changes associated with the fans [2]. Transient motion of the vehicle structure from road inputs also will excite the cooling module, inducing stresses within the radiator structures [2].

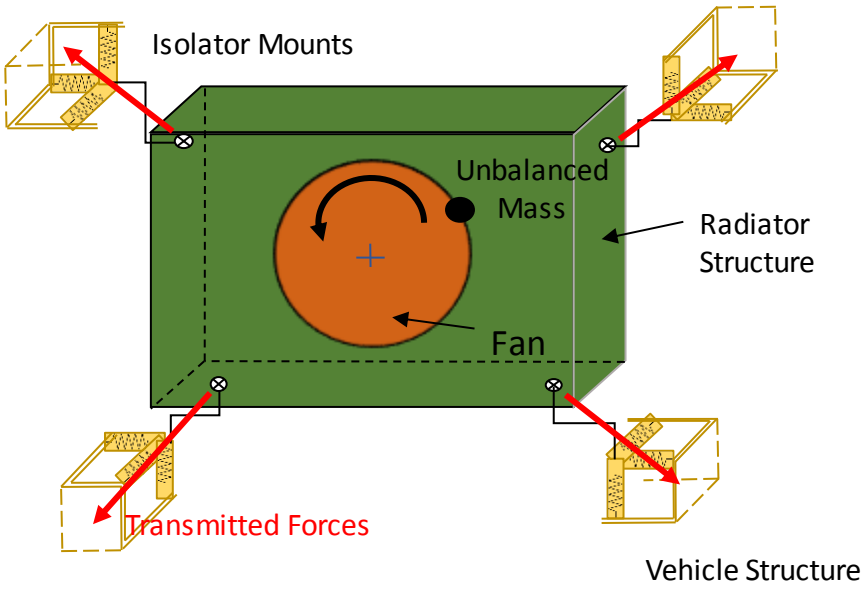

Figure 1. Example automotive cooling module system with radiator, isolator mounts, and fan.

There are more than 10,000 patents related to automotive radiator or cooling module isolation, but only few technical papers are published on this topic [3]. Traditional designs of cooling modules typically focus on packaging and layout demands, but not on a systematic way to address vibration and noise control [2, 4]. In the previous studies,

systems are usually modeled as a simple one-dimensional mass supported on springs to reduce complexity of the mathematical analysis [2, 4]. These types of models are insufficient to capture the realistic multi-dimensional load paths through the elastomeric mounts. In particular, powertrain isolation design is done using models with the full 6-degree-of-freedom (DOF) motions of the powertrain bodies [5, 6]. Therefore, models with adequate physics, incorporating complex loading from mounted components and multi-dimensional load paths must be developed to investigate potential isolation problems with current and future automotive cooling module designs.

1.2. Background

Consider a 1DOF system given in Figure 2, where *m* is the system mass, *k* is the isolator system stiffness, and *c* is the isolator system viscous damping, and *x* is the displacement of the mass. The isolator system typically consists of multiple mounts, which are required to support the mass of the system and constrain the motion in other axes. The transmitted force magnitude through an isolator system from a harmonic force input *f* with input amplitude F_0 is given by

$$F_T = \frac{F_0\sqrt{1+(2\zeta r)^2}}{\sqrt{(1-r^2)^2+(2\zeta r)^2}}, \qquad (1)$$

where $r = \omega/\omega_n$, with ω is the harmonic excitation frequency, $\omega_n = \sqrt{k/m}$ is the natural frequency of the system, and $\zeta = c/\sqrt{4km}$ is the system damping ratio. For system isolation, the stiffness values of the isolators are typically specified for a given mass and operating frequency to have a value of $r > \sqrt{2}$, as illustrated in Figure 3.

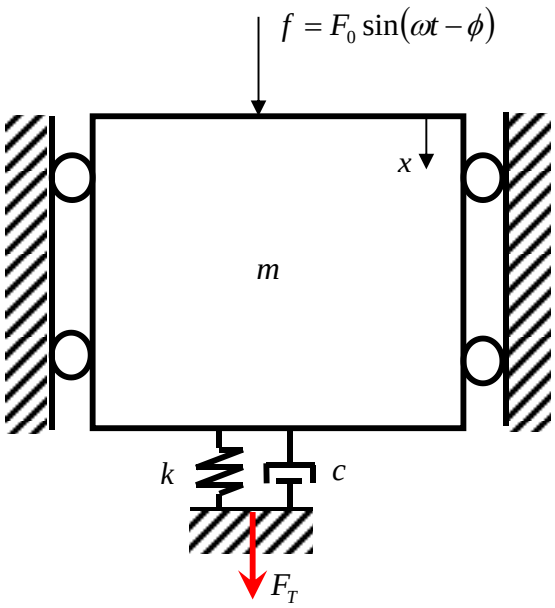

Figure 2. Schematic of forced vibration isolation problem.

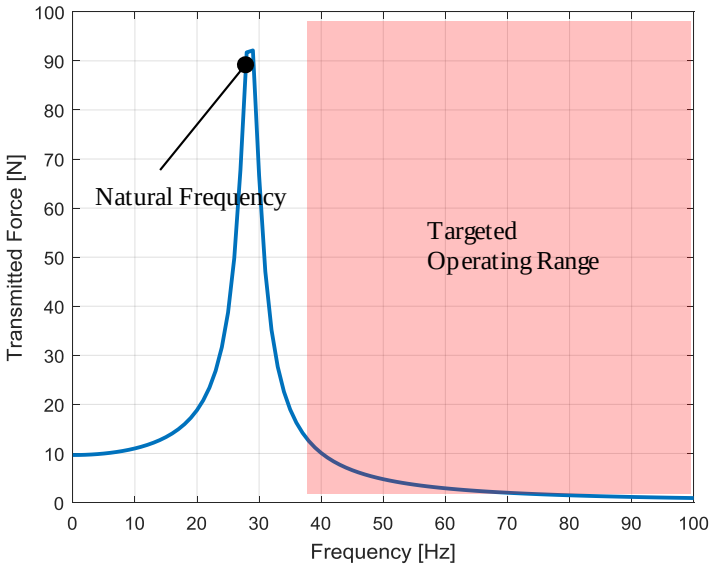

Figure 3. Example transmitted force from forced vibration problem with target operating range as isolation regime.

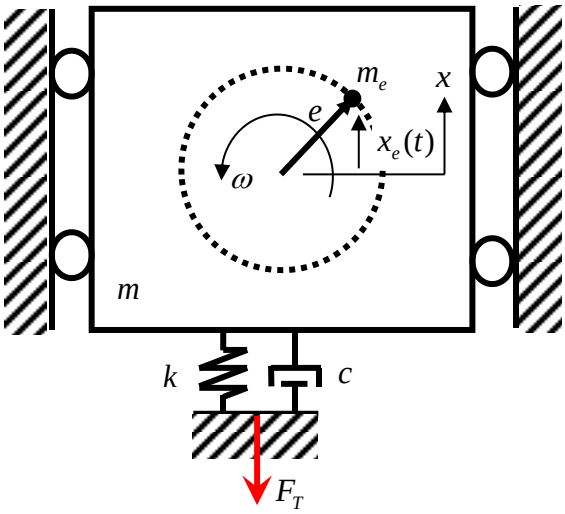

Figure 4. Schematic of simple rotating unbalance isolation problem.

For a rotating unbalance system, such as a fan, motor, engine, shown as a simple 1DOF system in Figure 4, the transmitted force magnitude through the isolator system is given by

$$F_T = \frac{m_e e k}{m} \frac{r^2 \sqrt{1+(2\zeta r)^2}}{\sqrt{(1-r^2)^2+(2\zeta r)^2}}, \qquad (2)$$

where m_e is an eccentric mass at radius of rotation e. For rotating unbalance systems, forces increase quadratically with frequency. Therefore, it is best for isolation to operate the system below the system's natural frequency, as illustrated in Figure 5. Typical electric fan speeds for large single fan radiator system range from 600 to 1800 rpm [13], with many fans operating well below 1200 rpm due to vibration and noise concerns. For higher order or higher speed vibration issues, the system may be desired to minimize transmitted force above the natural frequency, as done in the forced vibration problem.

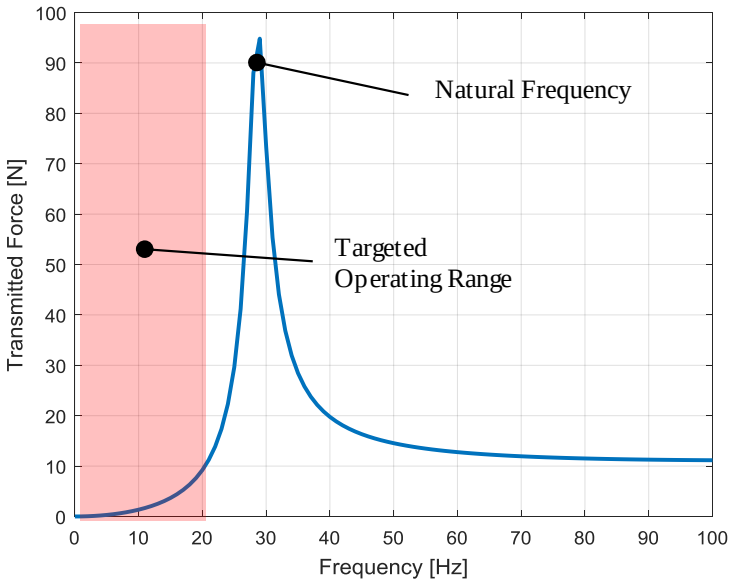

Figure 5. Example transmitted force from forced unbalanced problem.

The function of automotive cooling system is to remove heat from the vehicle combustion engine. Increasing the heat exchange efficiency of the radiator can yield better engine performance. Considering the heat exchange between the vehicle radiator and the ambient air by forced convection, the heat transferred per unit time is given by the equation

$$Q = hA_r(T_r - T_{air}), \qquad (3)$$

where h is the convective heat transfer coefficient, A_r is the effective surface area of radiator body, T_r is the temperature of radiator body, and T_{air} is the temperature of the ambient air.

In this heat transfer problem, the temperature of radiator body is affected by the vehicle engine, and it is assumed to be constant and at steady state. The temperature of air changes along with the outdoor weather, but it is not controllable by humans.

Therefore, the ways to improve the heat exchange between the radiator and the air include changing the convective heat transfer coefficient or changing the radiator surface area. In order to increase the radiator surface area, the volume and weight of the radiator usually have to be increased as well. However, the increased demand for lighter structure and compact vehicles often limits the applications of bigger and heavier radiators. The only way left to improve heat exchange is to increase the convective heat transfer coefficient. According to the relation between Nusselt number and convective heat transfer coefficient

$$Nu = \frac{hL}{k_{air}}, \qquad (4)$$

where L is the characteristic length of the radiator and k_{air} is the thermal conductivity of the air. From the equation, convective heat transfer coefficient increases as Nusselt number increases. Nusselt number is a function of Reynolds number. For a forced convection, Nusselt number has following approximately correlation with Reynolds number

$$Nu = \frac{0.3387\,\mathrm{Re}^{\frac{1}{2}}\,\mathrm{Pr}^{\frac{1}{3}}}{\left[1+\left(\frac{0.0468}{\mathrm{Pr}}\right)^{\frac{2}{3}}\right]^{\frac{1}{4}}}, \qquad (5)$$

where Re is the Reynolds number and Pr is the Prandtl number which is determined by properties of the fluid [14]. Nusselt number increases as Reynolds number increases. In

this case, Reynolds number increases with the velocity of the air across the radiator according to the equation

$$\mathrm{Re} = \frac{uL}{\nu}, \qquad (6)$$

where u is the velocity of the air, L is a characteristic linear dimension, and v is the kinematic viscosity of the air.

Overall, in order to increase the convective heat transfer coefficient, the air velocity needs to be increased. The way to increase the air velocity is to operate the radiator fan at a higher speed. However, according to the discussion above, when the system is operating below the natural frequency, increasing fan speeds will make the system close to the resonant frequency and have a larger transmitted force. For this specific problem, based on natural frequency equation of the 1DOF system, $\omega_n = \sqrt{k/m}$, the isolator system stiffness k should be modified to move the resonance to a higher frequency and improve the fan speed operational range.

2. Problem Formulation

The goal of this research is to evaluate and better understand the effects of the mounting layout on the dynamic response of an automotive cooling module subjected to vibratory excitations. Accordingly, a systematic study of a representative automotive cooling module isolation system is proposed. The study will be limited to dimensions of a commercially available radiator-fan assembly and to excitation frequencies below 100 Hz at which the radiator and support structure is assumed to be rigid. The steps to achieve the research goal are to:

(i) create a lumped parameter model of a radiator-fan assembly subjected to different mounting layouts;

(ii) identify elastomeric mount stiffness and damping matrices using a correlation between finite element analysis and dynamic bench experiments;

(iii) design and utilize a laboratory experiment to validate the model for specific cases;

(iv) exercise the model to quantify the isolation performance of the radiator-fan assembly with different isolator mount stiffness and damping properties as well as mounting locations.

To make this a tractable problem, this study will be restricted to the study of lower isolator mount modifications. The specific system has two lower isolators and two upper isolators. Due to the dimensions of the system, the study will be restricted to translational

and rotational motions within a single plane. The dynamic forces and deflections will be characterized about an operating point and will be assumed relatively small not to induce geometric nonlinearities into the system. Linear system principles will be assumed where the analysis will be conducted in the frequency domain. Constant stiffness and viscous damping coefficients will be assumed. The operating speeds of interest of this system will be restricted to 1200 rpm (20 Hz) or below, although dynamic response of the system will be characterized up to 100 Hz. First order rotating unbalance terms will only be considered. The isolator mounts will be considered the primary source of damping in the system. Damping of the isolator mounts will be scaled to match modal damping ratios calculated in bench experiments. Stiffness parameters will be derived to for realistic modifications of the system of interest.

The source of vibration considered in this study will be that of a rotating unbalance (inherent from mass production and assembly variation) due to a single fan mounted on the radiator structure. Hoses and other flanking attachments from the radiator body to the vehicle structure are also ignored. The outcome of this study will be to identify modifications to the current lower isolator mounts to expand the isolation performance at the maximum frequency of interests for this rotating unbalance problem. This work does not address other practical constraints the system may face, such as durability and crash performance.

3. Methodology

3.1. Lumped Parameter System Model (3DOF)

If the radiator vibration problem is restricted to analysis in the Y-Z plane, then the problem becomes 3DOF problem. The formation for a radiator body constrained by four elastic mounts is shown in the schematic in Figure 6. In this model, the operating point of the radiator body is defined by a rotational inertia in the Y-Z plane about the center of mass (denoted by subscripts of 0), given by a position vector $\vec{r}_0 = (y_o, z_o)$, where *y* and *z* are in units of meters. The deflection of the radiator body at the center of is given by a displacement vector $\Delta\vec{r}_0 = (\Delta y_o, \Delta z_o)$ and rotational vector $\Delta\vec{\phi}_0 = \Delta\theta_0$, where θ is in units of radians. For Mount 1 (denoted by subscripts of 1), shown in Figure 6, which is defined by a stiffness matrix of

$$\mathbf{K}_{c1} = \begin{bmatrix} \mathbf{K}_T & \mathbf{0} \\ \mathbf{0} & K_R \end{bmatrix} = \begin{bmatrix} k_{y1} & 0 & 0 \\ 0 & k_{z1} & 0 \\ 0 & 0 & k_{\theta 1} \end{bmatrix}, \qquad (7)$$

where k_y and k_z are the translational stiffness parameters in the Y- and Z-directions of the mount (in units of N/m), respectively, and k_θ is the rotational stiffness parameter (in units of Nm/rad) about the center of the mount, defined as (y_1, z_1). The translation stiffness terms are defined by a submatrix $\mathbf{K}_T$, and the rotational stiffness term is defined by a scalar K_R. The relative position vector between the center of mass and the mount center is

given by $\vec{r}_{01} = \left(y_1 - y_o, z_1 - z_o\right)$. Therefore, the displacement at the mount center is given by $\Delta\vec{r}_1 = \Delta\vec{r}_0 + \Delta\vec{\phi}_0 \times \Delta\vec{r}_{01}$, where $\times$ is the cross-product. The elastic forces at the mount center due to this displacement is given by $\Delta\vec{F}_1 = \mathbf{K}_{T1}\Delta\vec{r}_1$ and $\Delta\vec{M}_1 = K_R\Delta\vec{\phi}_0$, respectively. The moment (in N-m) induced at the center of mass due to the elastic constraints is given by $\Delta\vec{M}_0 = \vec{r}_{01} \times \Delta\vec{F}_1 + K_R\Delta\vec{\phi}_0$.

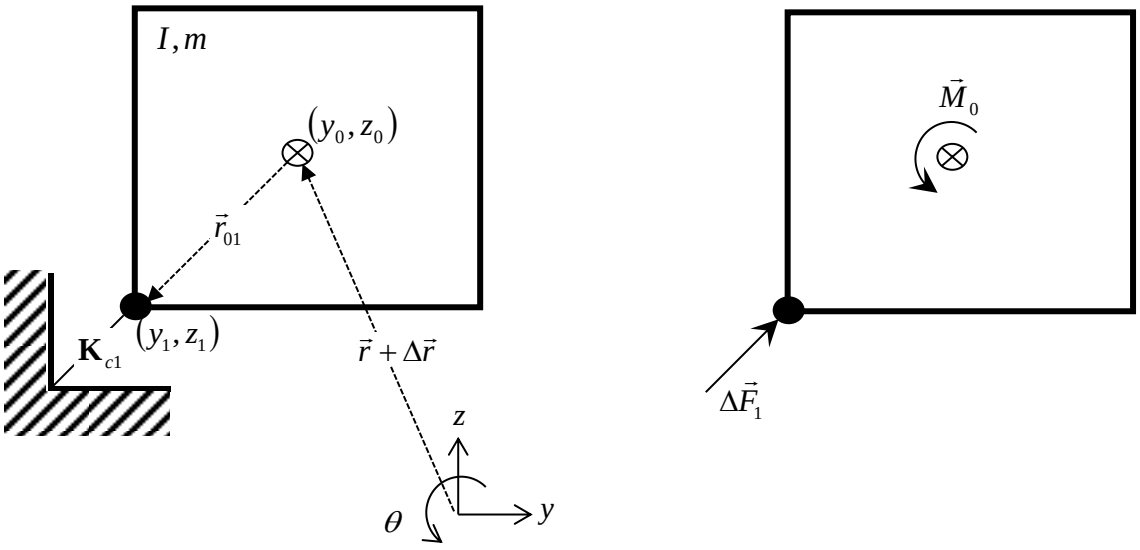

Figure 6. Schematic of 3DOF radiator vibration problem for one elastic mount.

If a displacement vector is defined as $\vec{q}_0 = \left[\Delta y_0 \quad \Delta z_0 \quad \Delta\theta_0\right]^{\mathrm{T}}$ and an elastic reaction force vector is defined as $\vec{R}_0 = \left[F_{y0} \quad F_{z0} \quad M_0\right]^{\mathrm{T}}$ about the center of mass, then the displacement vector and reaction force vector at the center of Mount 1 can be calculated by

$$\vec{q}_1 = \begin{bmatrix} \Delta y_1 \\ \Delta z_1 \\ \Delta\theta_1 \end{bmatrix} = \begin{bmatrix} 1 & 0 & (z_1 - z_0) \\ 0 & 1 & -(y_1 - y_0) \\ 0 & 0 & 1 \end{bmatrix} \begin{bmatrix} \Delta y_0 \\ \Delta z_0 \\ \Delta\theta_0 \end{bmatrix} = \mathbf{B}_{01}^{\mathrm{T}} \vec{q}_0 , \tag{8}$$

and

$$\vec{R}_0 = \begin{bmatrix} F_{y0} \\ F_{z0} \\ M_0 \end{bmatrix} = \begin{bmatrix} 1 & 0 & 0 \\ 0 & 1 & 0 \\ (z_1 - z_0) & -(y_1 - y_0) & 1 \end{bmatrix} \begin{bmatrix} F_{y1} \\ F_{z1} \\ M_1 \end{bmatrix} = \mathbf{B}_{01} \vec{R}_1 , \tag{9}$$

respectively, where the superscript T is a transpose operator and **B** are the respective coordinate transfer matrices. Thereby, the elastic reaction force vector at the center of Mount 1 is given by $\vec{R}_1 = \mathbf{K}_{c1}\vec{q}_1 = \mathbf{K}_{c1}\mathbf{B}_{01}^{\mathrm{T}}\vec{q}_0$, and the elastic reaction force vector about the center of mass is given by $\vec{R}_0 = \mathbf{B}_{01}\mathbf{K}_{c1}\mathbf{B}_{01}^{\mathrm{T}}\vec{q}_0$.

If a system is considered with four mounts, each with a mount center (y_i, z_i) denoted by subscript i = 1 to 4, then the total elastic reaction force at the center of mass will be given by $\vec{R}_0 = \left(\sum_{i=1}^{4} \mathbf{B}_{0i}\mathbf{K}_{ci}\mathbf{B}_{0i}^{\mathrm{T}} \right) \vec{q}_0$. By inspection, the effective stiffness about the center of mass due to the four mounts will $\mathbf{K}_0 = \sum_{i=1}^{4} \mathbf{B}_{0i}\mathbf{K}_{ci}\mathbf{B}_{0i}^{\mathrm{T}}$. Likewise, using the displacement vector convention, the inertia matrix defined about the center of mass will be given by

$$\mathbf{I}_0 = \begin{bmatrix} m & 0 & 0 \\ 0 & m & 0 \\ 0 & 0 & I \end{bmatrix}, \tag{10}$$

where m is the mass (in kg) and I is the rotational inertia (in kg-m^2) of the radiator. An assumed proportional damping matrix can be expressed for this system by $\mathbf{C}_0 = \beta \mathbf{K}_0$, where β is a scalar (in units of 1/s) determined by comparison to experimental results.

The normal mode natural frequencies and eigenvectors (e.g. mode shape vectors) of this 3DOF system can be obtained by solving the eigenvalue problem defined by $\left(-\omega_k^2 \mathbf{I}_0 + \mathbf{K}_0\right)\vec{\psi}_k = \vec{0}$, where $\vec{\psi}_k$ is the eigenvector and ω_k is the natural frequency (in rad/s) of the k^{th} mode.

3.2. Experimental Validation

An experiment is designed to validate the 3DOF system described earlier. In this experiment, a commercially available automotive cooling model, consisting of a radiator and mounts, is assembled vertically on a bedplate. The radiator is drained and tested empty with no hoses or fan assembly. The fixturing and radiator is assumed to be rigid (confirmed with natural frequencies much greater than those of the rigid-elastic body motions of interest). The propose of this experiment is to validate the 3DOF model proposed in the previous section. A modal impact test was conducted on the radiator. This test consisted of gluing four triaxial accelerometers (PCB 356A15, nominal sensitivity of 100 mV/g) to the radiator frame in its corners. A modal impact hammer (PCB 086C03, nominal sensitivity of 2.25 mV/N) was used to input an impulse load (for each run) at the upper corner of the radiator frame in the longitudinal (x), lateral directions (y), vertical (z), as illustrated in Figure 7.

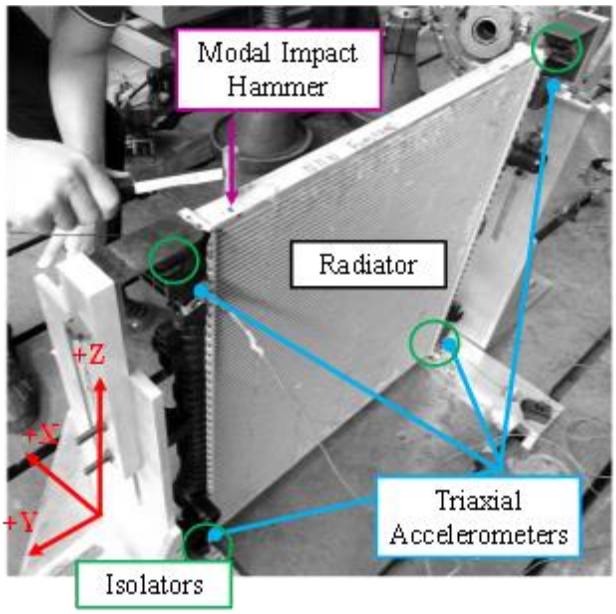

Figure 7. Cooling module isolation system modal experimental setup.

Each run consisted of five impacts, and the H_1-estimated frequency response functions with Force-Exponential windows were averaged. An additional three runs were conducted with the accelerometers glued to radiator frame at the mid-points between the corners on the outer edges. The data was analyzed using Siemens PLM LMS Test.Lab software with the PolyMax curve-fitter [9, 10]. From this analysis, the natural frequencies, modal damping ratios, and associated mode shapes were identified and recorded in a table. For the interest of this model, vertical, lateral, and rocking rigid body modes were identified. The results are given in Table 1.

Table 1. Modal experiment and model correlation.

Average $\zeta = 0.05$ for each mode (experimentally)

Lower Isolator Hardness [ShA]	Vertical Stiffness k_z [N/mm]	Lateral Mode Frequency [Hz]			Vertical Mode Frequency [Hz]			Rocking Mode Frequency [Hz]		
		Expt.	Model	Diff.	Expt.	Model	Diff.	Expt.	Model	Diff.
41	125	25.5	26.0	0.5	33.5	32.5	-0.5	57.0	57.0	0.0
49	180	28.0	29.0	1.0	40.5	38.5	-2.0	65.5	67.5	2.0
59	230	30.0	31.5	1.5	45.0	43.0	-2.0	73.0	76.0	3.0

Upper isolator: $k_y = 20$N/mm, kz = $0.5k_y$; k_θ (Nmm/rad) = $80k_z$

Lower isolator: $k_y = 0.7k_z$; k_θ (Nmm/rad) = $115k_z$

Each experiment was dissembled and re-assembled three times and was tested for three different lower mount hardness specifications. The average of the three repeated runs for each setup are reported. Approximately a +/-1 Hz variation was observed among repeated runs, which can be attributed to the assembly variation. In addition, a damping ratio was calculated using the PolyMax software for the runs. The average damping ratio observed for the different isolators was around 5%. This value will be used for analysis of the forced vibration problem in the next section. The first flexural mode of the radiator structure was identified to be over 120 Hz; therefore, assuming the body to be rigid below the highest 80 Hz rigid body mode was considered a reasonable assumption.

3.3. Parameter Identification

The mass *m* of the radiator body was measured using a weigh scale. Rotational mass moment of inertia of the radiator in the Y-Z plane about its center of mass is approximated (as a plate) by

$$I = \frac{1}{12} m\left(l_y^2 + l_z^2\right), \qquad (11)$$

where l_y and l_z are the major width and height of the radiator structure, measured using a measuring tape. The mass of the radiator was measured to be 6.5 kg, and the inertia was calculated to be 0.548 kg-m^2.

The vertical stiffness parameters were determined using a 1DOF experiment, where a known mass was placed on four identical radiator isolators (same hardness material specification), and a modal impulse test was conducted to identify the vertical natural frequency, illustrated in Figure 8. For this test, the mass was impacted directly along the vertical axis of the specimen. The dynamic stiffness of a single isolator in the vertical direction can be calculated by $k_{zi} = m_b \omega_i^2 / 4$, where m_b is the mass of the bench test rigid mass and ω_i is the natural frequency of this bench test in rad/s. This setup was done on the upper isolator as well as the four different lower isolator specifications.

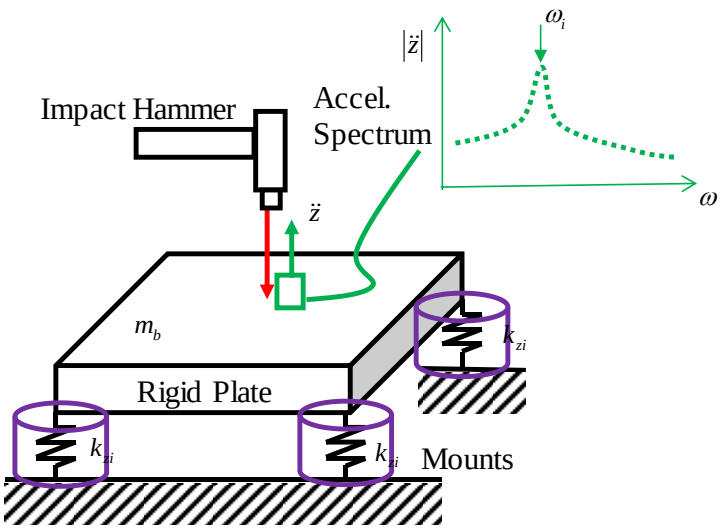

Figure 8. 1DOF mount stiffness identification modal experiment.

To obtain the off-axis stiffness parameters, i.e. k_{yi} and $k_{\theta i}$, a linear elastic finite element analysis was done. For this analysis, a solid model of each isolator was created in SolidWorks software [12], shown in Figure 9. The models were then imported into Abaqus CAE [11] and meshed with quadratic tetrahedral elements with maximum element size of 0.1 mm. Nominal linear elastic properties were assumed for the isolators (Young's modulus of 6 MPa and a Poisson's ratio of 0.49). The elements of the outer surfaces of the isolators were constrained to zero displacement and zero rotation conditions, illustrated in Figure 10. A reference point was created at the geometric center of each isolator. The inner surface of each isolator was tied to its respective reference point using a kinematic tie constraint, as shown in Figure 11.

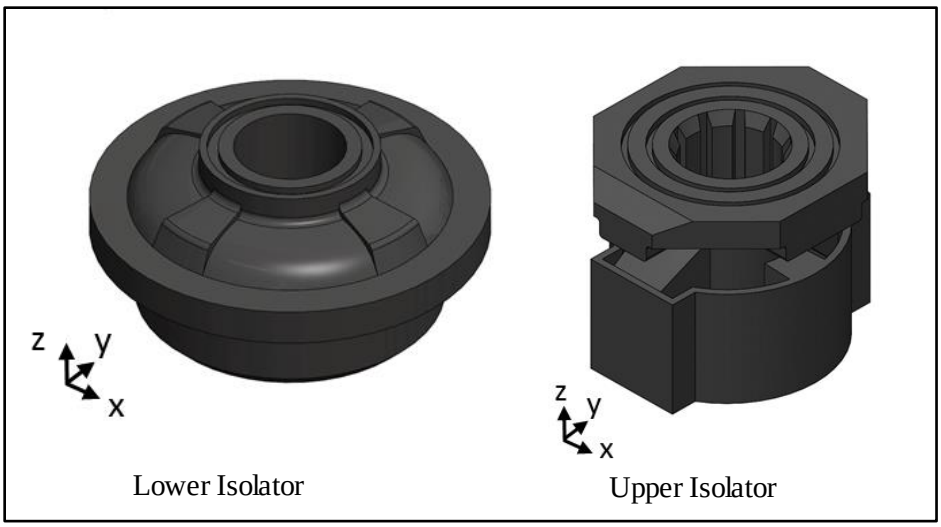

Figure 9. Solid model of lower and upper isolators.

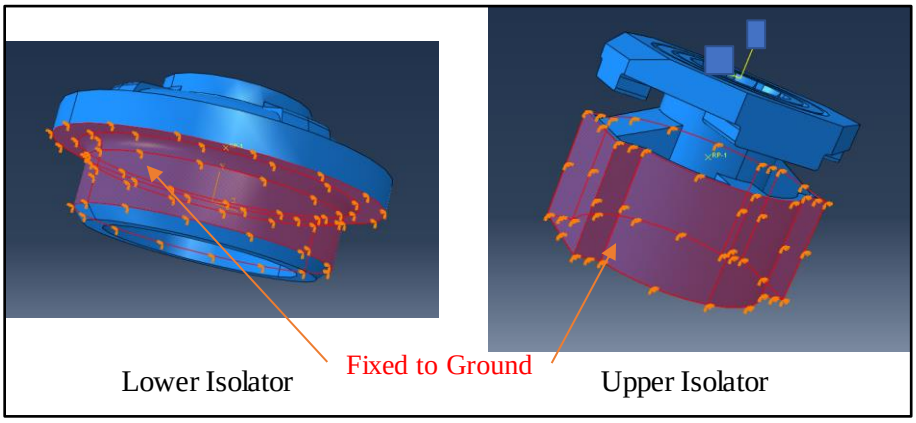

Figure 10. Outer constraint of finite element model.

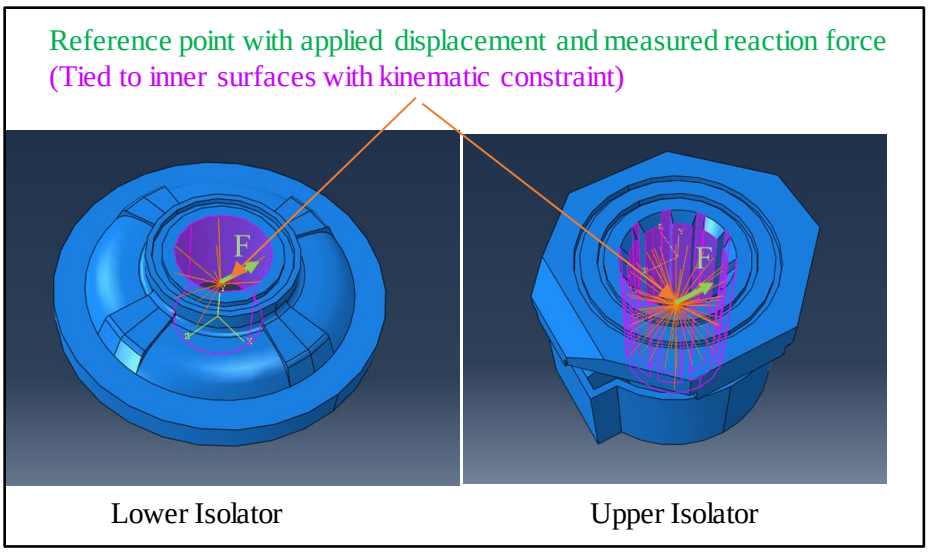

Figure 11. Inner constraint in finite element models.

A linear static perturbation analysis was performed with a unit (1 mm) displacement in a given direction. This was done for the Y- and Z- directions, and the stiffness (in N/mm) in each direction was calculated as the measured reaction force (in N) of the reference point in the respective direction. For the upper and lower isolators, the ratio of the k_y to k_z was calculated. This ratio was used to scale the values of k_z determined in the 1DOF mount stiffness identification experiments. Likewise, a unit angular displacement (0.001 rad) was applied to the reference point to estimate k_θ, and the measured reaction moment (in N-mm/rad) was calculated. These values were also scaled by the respective k_z for each mount. The resulting values of k_z and their off-axis scaling values are given in Table 1 in the previous section.

3.4. Model Correlation

Referring to Table 1, the difference between the natural frequencies for the three modes (lateral, vertical, and rocking) for the model and the experiment were compared. For each case with a different lower isolator stiffness (higher Shore A material hardness specification), the lateral mode was the lowest and the rocking mode was the highest. For the lateral mode, the model over-predicted by less than 1.5 Hz; for the vertical model, the model under-predicted by less than 2 Hz; and for the rocking mode, the model over-predicted by less than 3 Hz. The difference between model and experiment increased with higher stiffness isolator (higher material hardness specification). This is likely due to increased coupling between rotation and translational stiffness terms, not included in the model. Physically, this means the rotational center of the isolator mount may differ from the assumed geometric center of the isolator. When the stiffness increases, this difference becomes more significant. Another reason for disagreement between the model and the experiment could pertain to the simple inertia estimation using the major dimensions of the radiator frame. However, this error is not as likely to explain the differences observed since modifying this inertia in the model did not yield improved results. In addition, coupling of out-of-plane motions may also lead to disagreement, since the model assumed the motions in one plane. However, despite the observed deviation from model to experiment in these cases, this simple 3DOF model reasonably captured the behavior observed in the experiment. Thus, exercising the model parameters should provide some insight into modifications of the isolation performance of the system.

3.5. Rotating Unbalance Problem

For the system under operation in the vehicle, the fan mounted to radiator of the system is considered to provide a rotating unbalance input, defined by an eccentric mass m_e moving about a center of rotation at a constant radius of *e.* A schematic of this setup is given in Figure 12. Assuming a linear system, if the system is considered to operate at a given harmonic input, the where resulting motion would take the form $\vec{q} = \vec{q}_0 \cos(\omega_0 t - \phi)$, the forced excitation problem would be defined by

$$\left(-\omega_0^2 \mathbf{I}_0 + j\omega_0 \mathbf{C}_0 + \mathbf{K}_0\right)\vec{q}_0 \cos\left(\omega_0 t - \phi\right) = \begin{bmatrix} m_e e \omega_0^2 \cos\left(\omega_0 t\right) \\ m_e e \omega_0^2 \sin\left(\omega_0 t\right) \\ 0 \end{bmatrix}, \quad (12)$$

where ω_0 is the operating frequency in rad/s, ϕ is a phase angle in radians, *t* is time in seconds, and $j = \sqrt{-1}$.

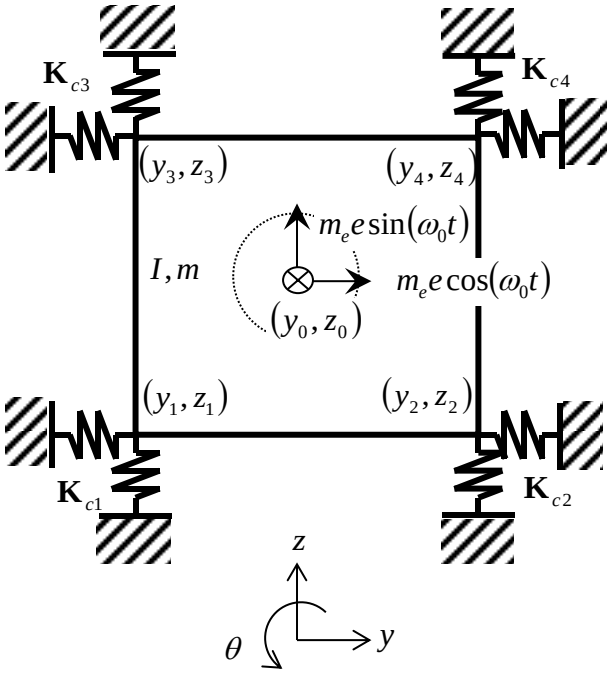

Figure 12. Schematic of equivalent system with rotating unbalance input transferred to the center of mass as a two-component vector.

For this analysis, the mass of the fluid inside the radiator was included as well as the mass of the fan. The mass of the fluid was approximated to double the mass of the radiator and the mass of the fan was estimated as 2.5 kg. A rotating unbalance of 1 g was applied to the assumed outer radius of the fan at 0.3 m. The mounts were placed at the original locations. The planer problem does not account for gyroscopic moments induced; however, the speeds considered are low enough for this assumption to be acceptable. Most of the system damping will be assumed to be attributed to the isolator mounts and will be tuned to a value of 5% modal damping by matching the peak value of the vertical mode to that of a 1DOF system. This model will be used in the next section to assess the vibration isolation performance of the system due to lower isolator modifications.

4. Analysis

In this section, the rotating unbalance model of the radiator system will be used to understand the effects of lower isolator mount modifications. First, the baseline radiator configuration will be evaluated changing only the stiffness of the lower isolators (uniformly scaled in each direction to represent a change in material hardness specification). For the next study, different locations of the high stiffness isolator mounts will be considered. Then, a change in damping of the lower isolator mounts will be evaluated. Finally, a change in lateral stiffness alone of the lower isolator mounts will be evaluated. The parameters used in these models and the different cases described are given in Table 2.

Table 2. List of model parameters for different cases.

Description		Parameter	Units	Modal Correlation			Rotating Unbalance						
				125 N/mm	180 N/mm	230 N/mm	125 N/mm	180 N/mm	230 N/mm	Case I	Case II	Case III	Case IV
Radiator Body	Mass	m	kg	6.5			15.5						
	Inertia	I	kgm^2	0.548			1.1492						
	Location	y0	mm	0			0						
		z0	mm	0			0						
Lower Isolator Mounts	Stiffness	ky	N/mm	88	126	161	88	126	161				230
		kz	N/mm	125	180	230	125	180	230				
		kt	Nm/rad	14	21	26	14	21	26				
	Damping	b	1/s	0.0015			0.0015					0.003	0.0015
	Location	y1	mm	-381			-381			-191	-381		
		z1	mm	-355			-355						
		y2	mm	381			381			191		-381	
		z2	mm	-355			-355						
Upper Isolator Mounts	Stiffness	ky	N/mm	20									
		kz	N/mm	10									
		kt	Nm/rad	0.760									
	Damping	b	1/s	0.0015									
	Location	y3	mm	-381									
		z3	mm	355									
		y4	mm	381									
		z4	mm	355									

4.1. Change in Lower Isolator Material Hardness Specification

As shown in the previous section, the change in the isolator hardness yields a scaled increase in both k_y and k_z. The material used for these radiator mounts are ethylene propylene diene monomer (EPDM). Variations in hardness of this rubber due to processing conditions effectively changes the elastic modulus of the material. No changes in damping properties due to hardness changes were observed in the modal experiments in the previous section. Figure 13 shows the total peak-to-peak lateral force (F_{y0}), vertical force (F_{z0}), and moment (M_0) at the center of mass of the radiator body for the 125 N/mm lower isolator mounts at different operating frequencies. Figure 14 shows the peak-to-peak lateral force (F_{yi}), vertical force (F_{zi}), and moment (M_i) through each of the isolator mounts for the same system. The total vertical force is higher than the lateral force, and its peak occurs at a slightly higher frequency, as suggested by the modal analysis in the previous section. The forces are about five times higher through the lower isolator mounts than the upper isolator mounts. The lower isolator mounts are dominated by the vertical force contribution, while the upper mounts are dominated by the lateral force contribution. The moments transfer through the mounts are minimal (<<1 N-m) for each case. Due to the combination of the moment and forces, Mount 1 has slightly higher forces transferred through it (~10%). The 180 N/mm and 230 N/mm mounts exhibit similar force and moment spectral characteristics as shown in Figures 13 and 14; therefore, for brevity, they have been omitted.

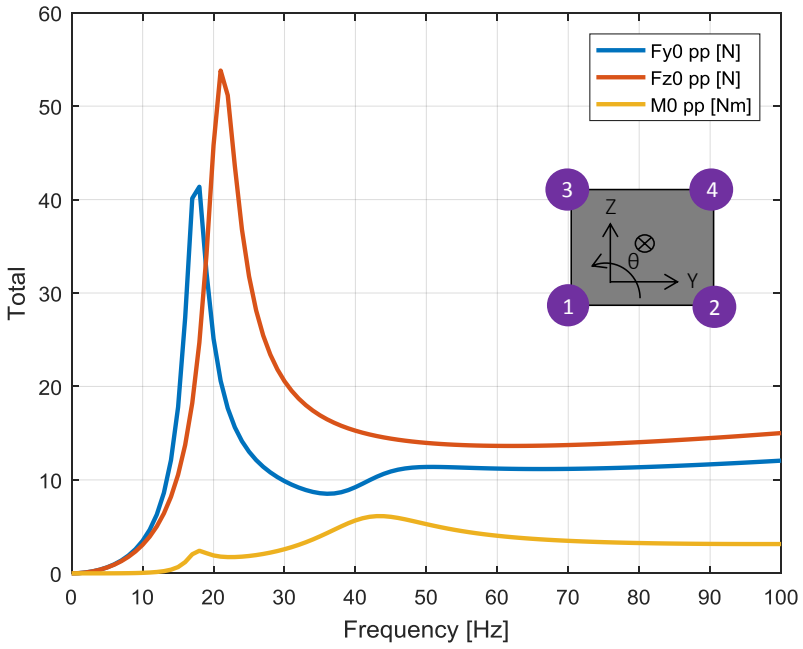

Figure 13. Total peak-to-peak lateral force (F_{y0}), vertical force (F_{z0}), and moment (M_0) at the center of mass of the radiator body for the 125 N/mm lower isolator mounts at different operating frequencies.

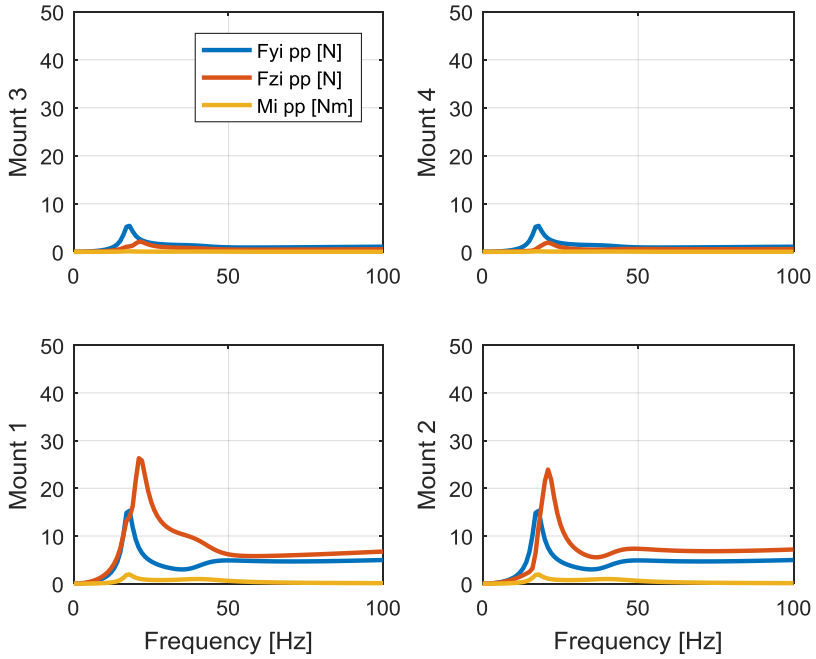

Figure 14. Peak-to-peak lateral force (F_y), vertical force (F_z), and moment (M) at each mount for the 125 N/mm lower isolator mounts at different operating frequencies.

Figure 15 shows the change in lateral, vertical, and rocking modes due to lower mount stiffness modification. As expected, the natural frequency of each mode increases as the lower mount stiffness increases. The lowest natural frequency observed is around 18 Hz for the lateral mode, attributed to the lowest stiffness mounts. The total change in lateral natural frequency over the stiffness range considered is 4 Hz; the total change in vertical natural frequency is 8 Hz; and the total change in rocking natural frequency is 16 Hz. This suggests that the rocking natural frequency is much more sensitive to changes in lower mount stiffness.

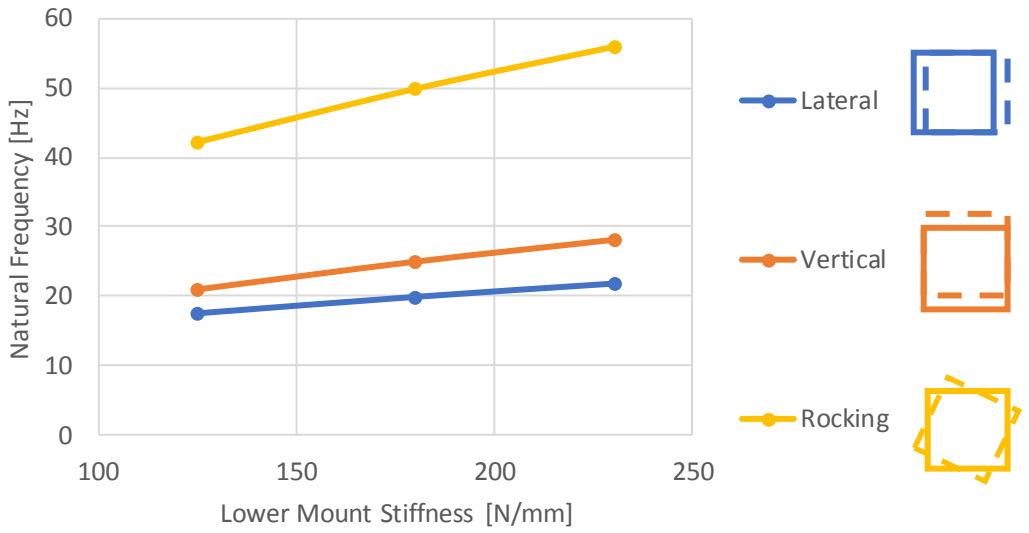

Figure 15. Change in lateral, vertical, and rocking modes due to lower mount stiffness modification.

To compare the vibration isolation performance of each system, the force and moment responses at the maximum speed of interest of 1200 rpm (20 Hz) was calculated. As can be observed in these spectra, the forces and moments transmitted increase quadratically with frequency, with peaks occurring at the natural frequencies of the system. Since the lowest natural frequency of the system occurs near 20 Hz, the isolation performance should be adequately quantified. Figure 16 shows the peak-to-peak forces and moments at 20 Hz for the different lower isolator stiffness cases. As in Figure 14, the lower isolators had the greatest forces transmitted. Overall, the lowest vertical force transmitted were attributed to the 230 N/mm lower isolator mounts. The lowest lateral forces transmitted were attributed to the 125 N/mm lower isolator mounts. Figure 17 shows the total peak-to-peak force and moments at the center of the mass of the radiator body at 20 Hz for the different mount cases. Likewise, the lowest vertical forces are attributed to

the 230 N/mm lower isolator mounts, and the lowest lateral forces are attributed to the 125 N/mm lower isolator mounts.

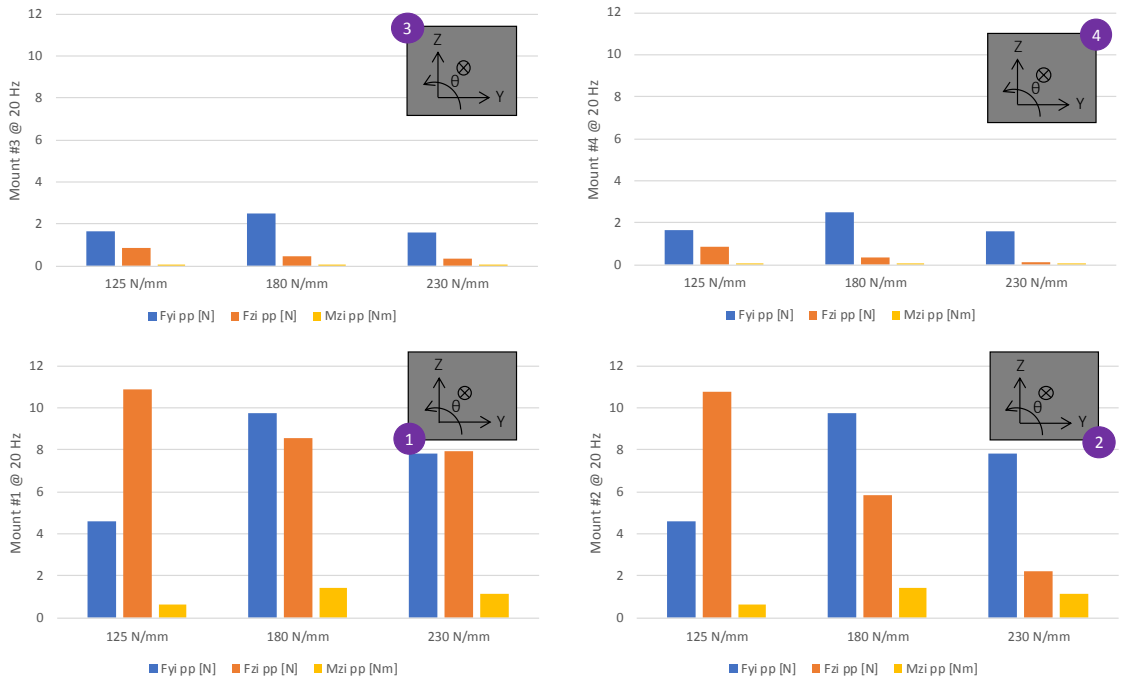

Figure 16. Peak-to-peak lateral force (F_y), vertical force (F_z), and moment (M) at each mount at 20 Hz for 125, 180, and 230 N/mm lower isolator mounts.

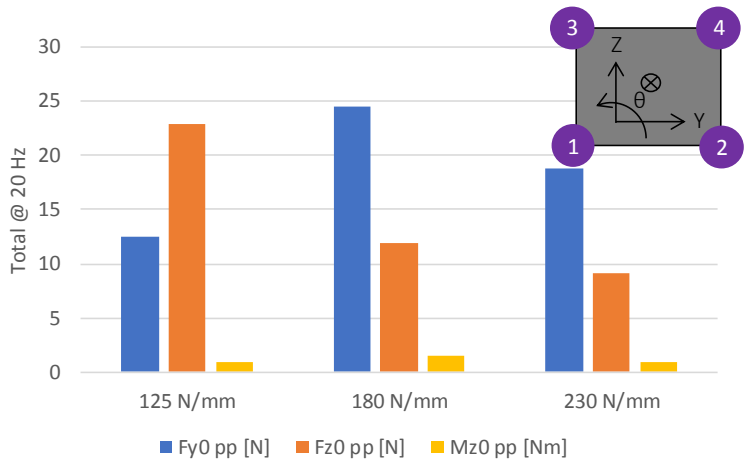

Figure 17. Total peak-to-peak lateral force (F_{y0}), vertical force (F_{z0}), and moment (M_0) at the center of mass of the radiator body at 20 Hz for 125, 180, and 230 N/mm lower isolator mounts.

4.2. Change in Lower Isolator Lateral Mount Center

The next study was done to evaluate the effect of a change in isolator position. In this study, the 230 N/mm lower isolator mounts were considered. The nominal condition was considered with the isolators at the outer edge of the radiator; Case I considered moving both lower isolators inward along the lateral (Y) axis towards the center of the radiator; and Case II considered moving only one of the lower isolators inward along the lateral axis towards the center of the radiator. Figure 18 shows the effect of these changes on the natural frequencies of the system. For the different cases, the vertical and lateral natural frequencies remain relatively unchanged. As the mounts are moved closer together, the rocking natural frequency decreases, as expected.

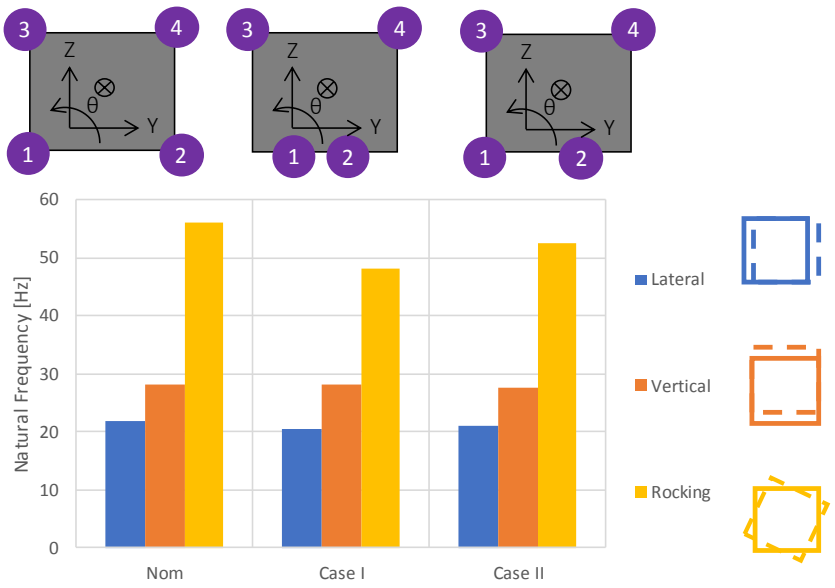

Figure 18. Change in lateral, vertical, and rocking modes due to lower mount location modification for the 230 N/mm lower isolator mounts.

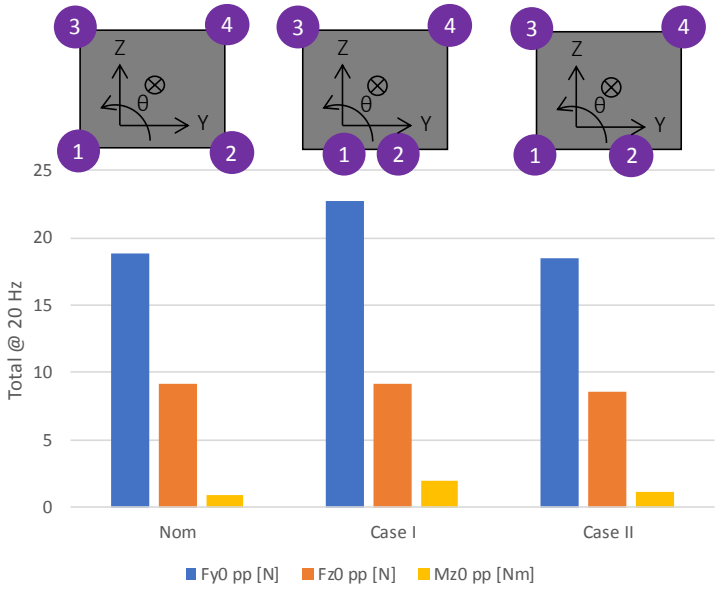

Figure 19. Total peak-to-peak lateral force (F_{y0}), vertical force (F_{z0}), and moment (M_0) at the center of mass of the radiator body at 20 Hz for 230 N/mm lower isolator mounts at different lateral positions.

Figure 19 shows the total peak-to-peak forces and moments at the center of mass of the radiator body for the 230 N/mm lower isolator mounts at different lateral positions. Case I shows that moving the mounts closer together increases the total lateral forces transmitted in the system, likely due to the decrease in rotational stiffness of the system about its center of mass. The lower rotational stiffness also explains to lower rocking natural frequency of the system.

4.3. Change in Lower Isolator Mount Damping

In the next study, the effect of material damping changes to the lower isolator mount was investigated. For this study, the damping was doubled to approximately 10% modal damping for the 230 N/mm isolator mounts in the nominal positions. Figure 20 shows the total peak-to-peak forces and moment at the center of mass of the radiator body for this increased damping case (Case III). In contrast to Figure 13 for the nominal damping case (albeit for a lower stiffness mount), the shape of the curve has changed with a more pronounced increase as frequency increases. Figure 21 shows the total peak-to-peak forces and moment at the center of mass of the radiator body at 20 Hz for these two cases. The increased damping decreases the forces in the lateral direction by nearly 40%, while the vertical forces and moment are relatively unchanged. This is likely due to the proximity of the lateral natural frequency to 20 Hz, where damping will be most effective at reducing transmitted forces.

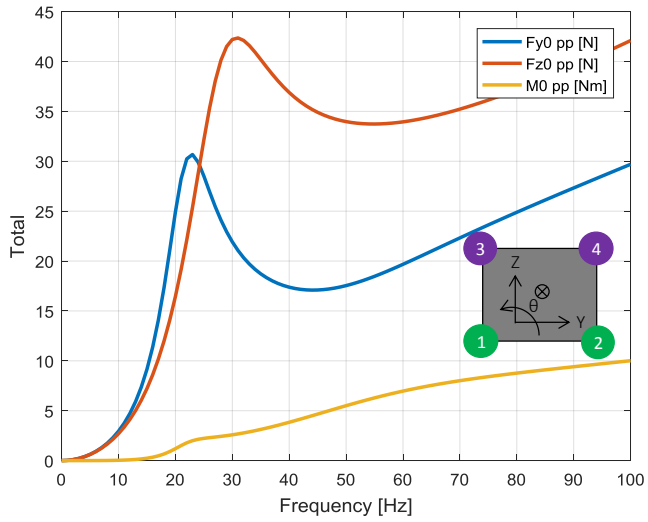

Figure 20. Total peak-to-peak lateral force (F_{y0}), vertical force (F_{z0}), and moment (M_0) at the center of mass of the radiator body for the 230 N/mm lower isolator mounts with higher material damping.

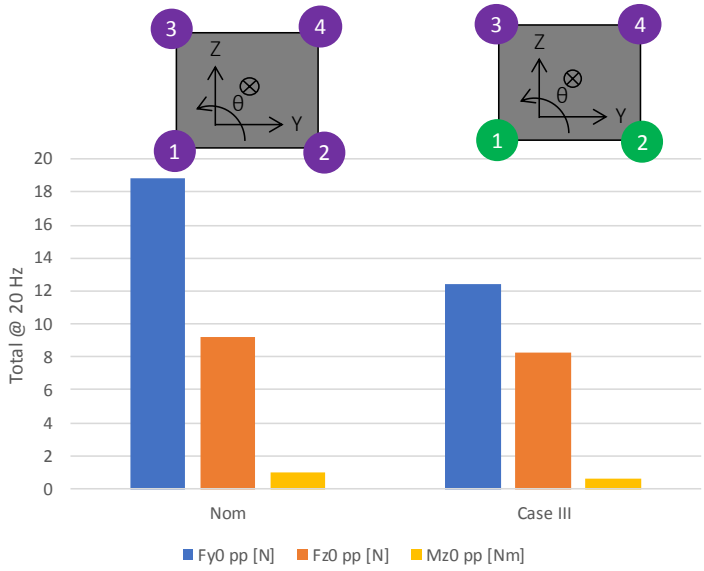

Figure 21. Total peak-to-peak lateral force (F_{y0}), vertical force (F_{z0}), and moment (M_0) at the center of mass of the radiator body at 20 Hz for 230 N/mm lower isolator mounts with different damping.

4.4. Change in Lower Isolator Lateral Stiffness

The final case considered was a change in lateral stiffness of the lower isolator mounts. Changing hardness without geometry changed both the vertical and lateral stiffness by the same proportion. However, if a change in geometry of the mount is considered, such as a smaller diameter mount with less vertical height, then the lateral stiffness would be increased, and the vertical stiffness could be maintained. Figure 22 shows the change in natural frequencies of the system from the nominal case (k_z =230 N/mm, k_y = 161 N/mm) to Case IV with a larger lateral stiffness (k_z = k_y = 230 N/mm). Case IV shows an increase in lateral and rocking natural frequencies of 1 Hz and 4 Hz, respectively, with no change in vertical natural frequency. Figure 23 shows the effect of the increase of lateral stiffness on the total peak-to-peak forces and moment at the center of mass of the radiator body at 20 Hz. Case IV with the increased lateral stiffness reduces the lateral forces and moment without affecting the vertical forces. If a reduction in both vertical and lateral forces is desired, changing the geometry of the mount may be needed.

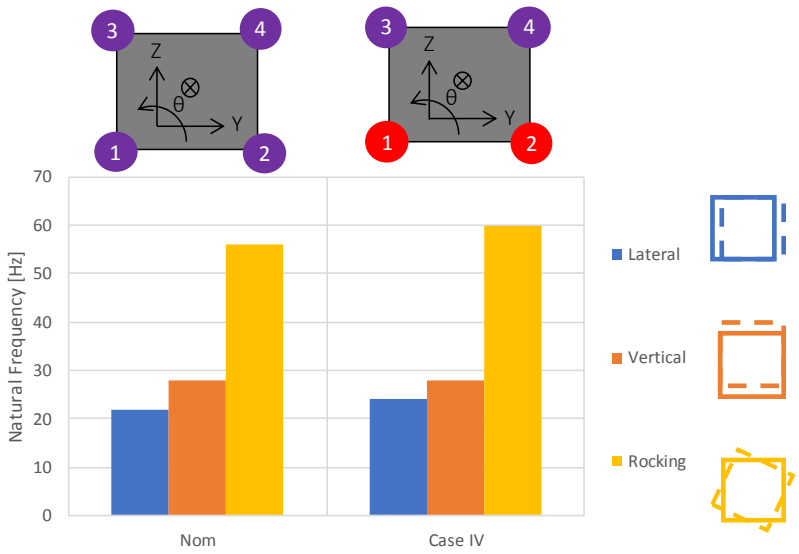

Figure 22. Change in lateral, vertical, and rocking modes due to increase in lateral stiffness (Case IV).

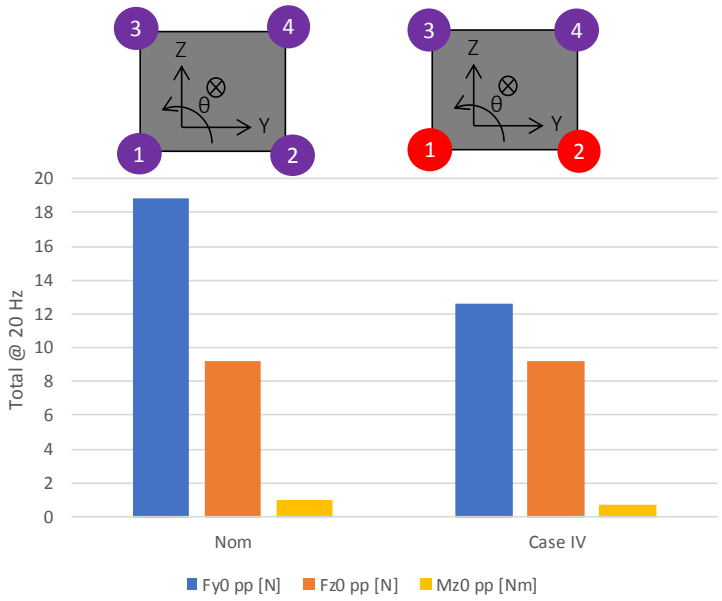

Figure 23. Total peak-to-peak lateral force (F_{y0}), vertical force (F_{z0}), and moment (M_0) at the center of mass of the radiator body at 20 Hz for nominal and increased lateral stiffness cases.

5. Conclusions

5.1. Summary

In this thesis, a lumped parameter model of a radiator-fan assembly is developed. The parameters of the model are identified by using the finite element analysis and dynamic bench experiments. The model is correlated to a modal experiment of a commercially available radiator structure constrained by four isolator mounts. The correlated model was then modified to evaluate a radiator structure with fan assembly which provided a nominal rotating unbalance input to lumped parameter model. Finally, the isolation performance of the radiator-fan assembly is evaluated for different lower isolator mount stiffness, damping, and positions.

5.2. Major Conclusions

For the radiator considered, the reductions of overall transmitted forces could be achieved through modifying the stiffness of lower isolator mounts. The dominant path for the force transmission is through the lower mounts. Increasing the stiffness of the lower mounts by increasing the rubber hardness increases stiffness in all directions. This increased stiffness lowers transmitted vertical forces before 20 Hz by pushing the vertical natural frequency upwards. However, lowering the stiffness lowers the transmitted lateral forces below 20 Hz. As discussed in the results, the trends of transmitted forces and isolator properties are different between the upper isolators and lower isolators. Moving the lateral position of the lower isolator mounts towards the center of the radiator also increases the

lateral forces transmitted, with no change in vertical forces transmitted. Increasing the damping of the mounts through a material change also decreases the forces transmitted, especially at modes near the operating frequency. Finally, increasing the lateral stiffness of the isolator mount while maintaining the same vertical stiffness, through a geometric change of the mount, also decreases the lateral forces transmitted by effectively shifting the lateral natural frequency upwards outside the operating range.

To recommend a modification to the isolation system, the vibration transmission sensitivity at the body-side structure of the mounts must be known (for example, quantified through a multi-dimensional transfer function of input acceleration or force at the mount location on the body-side structure to output acceleration on the driver seat structure). If the structural path from the lower mount to the driver is highly sensitive in the vertical direction, then this direction should be prioritized, leading to a suggested increase in rubber hardness. Conversely, if the structural path from the lower mount to the driver is highly sensitive in the lateral direction, then this direction should be prioritized, leading to a suggested increase in lateral stiffness of the mounts or change. There will also be a benefit if a higher damping isolator mount material or device (such as a hydraulic mount or shock absorber) can be employed.

5.3. Future Work

This lumped parameter model provides some insight into modifications to the lower isolator mounts to improve vibration isolation performance; however, the model considered in this study was limited to linear analysis and planar motion. To evaluate the

potential interactions with out-of-plane forces and motions, a multibody dynamics model should be used. The multibody dynamics model will also provide a means to evaluate transient and time domain phenomena.

In addition, the radiator body and support structures cannot be considered perfectly rigid, and their flexural modes may influence the forces transmitted through the isolator mounts. The rubber components are assumed to be linear, although rubber often exhibits amplitude and frequency dependency. Therefore, higher fidelity viscoelastic material models should be considered for the rubber components. There also may be some geometric nonlinearities due to clearances and multi-stage springs, which are often intentionally or unintentionally designed into the components or the assembly. Nonlinear stiffness elements should be included in the multibody model to capture these behaviors if they are identified through bench experiments.

Additionally, other radiator assemblies should be evaluated, such as those with dual fans and the addition of hoses or intercoolers. The effectiveness of isolation for higher order unbalances should be evaluated, as well as phasing among different sources on fan blades or multiple fans.

Additional experimental work could be conducted to validate the models in this thesis, such as applying a known rotating unbalance to the system and evaluating the system motion. The forces through the mounts could also be quantified using transfer path analysis, where the dynamic mount stiffness properties are measured using a bench test and the forces transmitted through the mounts on the assembled radiator structure are calculated using these stiffness properties and measured relative motion across the mounts. Preload and inertia estimation effects could also be evaluated by changing the mass

properties of the radiator through the addition of ballast masses at specific locations on the radiator body.

References

[1] Birch S., "Beware the NVH pitfalls of weight reduction," Automotive Engineering, 14 May 2013, Retrieved from <http://articles.sae.org/12154/>.

[2] Park, C.H., Shim, H.J., Choi, D.H., Kim, J.K., and Lee, S.M., "Shape optimization of rubber isolators in automotive cooling modules for the maximization of vibration isolation and fatigue life," International Journal of Automotive Technology, 13(1), 61-75, 2012.

[3] Google Scholar, Article / Patent Search, 1 February 2017, Retrieved from <scholar.google.com>.

[4] Lewitzke, C. and Lee, P., "Application of elastomeric components for noise and vibration isolation in the automotive industry," SAE Technical Paper 2001-01-1447, 2001.

[5] Erdelyi, H., Roesems, D., Toso, A., and Donders, S., "Powertrain mounting system layout for decoupling rigid-body modes in the vehicle concept design stage," SAE Technical Paper 2013-01-1706, 2013.

[6] Jeong T. and Singh R., "Analytical methods of decoupling the automotive engine torque roll axis," Journal of Sound and Vibration, 234(1), 85-114, 2000.

[7] MATLAB 2015b, Computer software, Mathworks, Inc., 2016, Retrieved from <http://www.mathworks.com/products/matlab/>.

[8] Kim S. and Singh R., "Multi-dimensional characterization of vibration isolators over a wide range of frequencies," Journal of Sound and Vibration, 245(5), 877-913, 2001.

[9] Peeters B., Lowet G., Van der Auweraer, H., and Leuridan, J., "A New Procedure for Modal Parameter Estimation," Sound and Vibration, 25-28, 2004.

[10] LMS Test.Lab 16, Computer software, Siemens PLM, Inc., 2017, Retrieved from <https://www.plm.automation.siemens.com/en/products/lms/testing/test-lab/>.

[11] Abaqus CAE 2013, Computer software, Dassault Systemes, Inc., 2017, Retrieved from <https://www.3ds.com/products-services/simulia/products/abaqus>.

[12] SOLIDWORKS 2017, Computer software, Dassault Systemes, Inc., 2017, Retrieved from < http://www.solidworks.com>.

[13] JEGS Automotive Parts, Retrieved Nov. 12, 2017 from <http://www.jegs.com/>.

[14] Incropera, F.P., DeWitt, D.P., Bergman, T.L., and Lavine, A.S., Introduction to Heat Transfer, 5th Edition, New York: John Whiley and Sons, 2007.